Cr cluster characterization in Cu-Cr-Zr alloy after ECAP processing and aging using SANS and HAADF-STEM

K. Abib, H. Azzeddine, B. Alili, L. Litynska-Dobrzynska, A. Helbert, T. Baudin, P. Jégou, M. Mathon, P. Zieba, D. Bradai

Cr cluster characterization in a Cu-Cr-Zr alloy after ECAP processing and aging using SANS and HAADF-STEM

K. Abib[1], H. Azzeddine[1,2*], B. Alili[1], L. Litynska-Dobrzynska[3], A.L. Helbert[4], T.Baudin[4], P. Jegou[5], M.H. Mathon[5], P. Zieba[3], D. Bradai[1]

[1]Faculty of Physics, University of Sciences and Technology Houari Boumediene, BP 32 El Alia, Bab Ezzouar, Algiers, Algeria

[2]Departments of Physics, University of Mohamed Boudiaf, M'sila, Algeria

[3]Institute of Metallurgy and Materials Science Polish Academy of Sciences, 25 Reymonta St., 30-059 Krakow, Poland

[4]ICMMO, SP2M, Univ. Paris-Sud, University Paris-Saclay, UMR CNRS 8182, 91405 Orsay Cedex, France

[5]Laboratoire Léon Brillouin, CEA-CNRS, CEA/Saclay, 91191 Gif-sur-Yvette, France

* Corresponding author: azehibou@yahoo.fr

Abstract

The precipitation of nano-sized Cr clusters was investigated in a commercial Cu-1Cr-0.1Zr (wt.%) alloy processed by Equal-Channel Angular Pressing (ECAP) and subsequent aging at 550 °C for 4 hours using small angle neutron scattering (SANS) measurements and high-angle annular dark-field– scanning transmission electron microscopy (HAADF-STEM). The size and volume fraction of nano-sized Cr clusters were estimated using both techniques. These parameters assessed from SANS (d~3.2 nm, F_v~1.1 %) agreed reasonably with those from HAADF-STEM (d ~2.5 nm, F_v~2.3%). Besides nano-sized Cr clusters, HAADF-STEM technique evidenced the presence of rare cuboid and spheroid sub-micronic Cr particles about 380-620 nm mean size. Both techniques did not evidence the presence of intermetallic Cu_xZr_y phases within the aging conditions.

Keywords: Cr-cluster; Precipitation; ECAP; Cu-Cr-Zr alloy; SANS; HAADF-STEM

1. Introduction

Cu-Cr-Zr alloys are the subject of many research activities owing to their potential use in industrial and technological areas such as electric/microelectronics and nuclear fusion reactors [1]. The high conductivity of these alloys is mainly attributed to the low solubility of Cr and Zr in copper at room temperature [2], while their strength is due to the precipitation of Cr clusters and Cu_xZr_y phases in copper matrix [3, 4]. However, many authors reported antagonist findings about the sequence and nature of precipitates that can appear during annealing after conventional or severe plastic deformation of Cu-Cr-Zr alloys [5–16]. Besides Cr clusters, different Cu_xZr_y phases were found in Cu–Cr–Zr alloys: orthorhombic Cu_4Zr phase [10, 17], $Cu_{51}Zr_{14}$ (believed to be Cu_3Zr) phase [11]. More complicated phases such as Cu_7Cr_3ZrSi, as well as $CrCu_2$(Zr, Mg) Heusler phases were also evidenced [18–20]. It was reported in binary Cu–Cr, Cu–Zr and ternary Cu–Cr–Zr alloy that Cr precipitates appeared first at about 440 °C and then Cu_3Zr precipitation occurred separately at about 520 °C [21]. Similar sequence where reported in Cu-Cr-Zr alloys severely deformed by equal angular channel pressing (ECAP) [5, 22].

The substantial influence of severe plastic deformation (SPD) such as ECAP or high-pressure torsion (HPT) on the structure, precipitation sequence, thermal stability and mechanical properties of Cu-based alloys has been the object of many studies [5, 21–29]. In fact, the processing of alloys by SPD is known to produce significant grain refinement and high density of dislocations and vacancies [30]. This will enhance the mobility of solute species and generate more nucleation sites for precipitations and consequently strongly modify their kinetics [24, 30].

After ECAP processing, the grains of Cu-Cr-Zr alloys underwent a strong refinement down to 1 µm concomitant with high dislocations densities and significant hardness enhancement up to 250 % [5, 22, 23, 27, 31]. Purcek et al. [27, 31] have shown that among the different ECAP

routes, route Bc was found to generate the lowest grain size, the highest hardness and strength [27]. It has been shown that post-ECAP aging led to a precipitation hardened ultra-fine grain structure rather stable under both thermal and mechanical influence [5].

Since the pioneer work of Vinogradov et al. [5], very few works have been devoted to the chemical and microstructural changes as well as to the precipitate nature and morphology, and to the sequence of the precipitation that may occur during and/or after SPD processing of Cu-Cr-Zr alloys.

Hatakeyama et al. [18], Chbihi et al. [32] reported quantitative data of size distribution, volume fraction and other morphological features of Cr clusters in Cu–Cr–Zr alloys without any prior deformation by using TEM and 3D-atome probe tomography (3D-ATP). They evidenced the existence of nanoscaled Cr precipitates with spherical, plate and ellipsoid shapes and sizes ranging between 2 and 50 nm.

Small Angle Neutron Scattering (SANS) and High-Angle Annular Dark-Field (HAADF-STEM) are powerful tools to determine the size distribution and volume fraction of the precipitates in materials and alloys. In contrast to microscopic techniques SANS analyzes a relatively large volume and thus provides average values over a very large number of precipitates, which makes it very sensitive to small changes in the size and volume fraction of precipitates [33].

The present study aims to evaluate, in a comparative way, the size distribution and the volume fraction of precipitates in a Cu-1Cr-0.1Zr (wt. %) alloy after SPD processing by ECAP and aging at 550 °C for 4h using SANS and HAADF-STEM techniques.

2. Experimental Procedure

The material considered in this study is a commercial Cu-1Cr-0.1Zr (wt. %) alloy that was supplied in the form of rod bars by Goodfellow (UK). Billets of 10 mm diameter and 60 mm

length were then machined for ECAP processing and solution heat-treated for 1 h at 1040 °C in a protective inert gas atmosphere followed by a subsequent water quenching. The rods were then processed by ECAP at room temperature up to 1 pass using route B_c. The full details of the ECAP processing can be found in references [34, 35]. This route was especially chosen to generate a fine equiaxed microstructure with a high volume fraction of high-angle grain boundaries [31]. After ECAP processing, annealing was carried out at 550 °C for 4 h under high vacuum.

Analytical transmission electron microscope FEI Tecnai G^2 at 200 kV equipped with high-angle annular dark field scanning transmission electron microscopy detector HAADF-STEM and an energy dispersive X-ray EDAX spectrometer (EDS) was employed for microstructural (ultrafine grain size, precipitate size distribution, their nature and volume fraction) characterization of the Cu-1Cr-0.1Zr alloy after various heat treatments. The TEM specimens were electro-polished using a Tenupol 5 twinjet polishing unit with an electrolyte of 75% CH_3OH and 25% HNO_3. In HAADF-STEM experiments the spot size 6 has been used (beam diameter about 1 nm). The volume fraction of the precipitates was estimated using Scion Image for Windows software. The area values of a selected number of precipitates in a TEM micrograph were computed and divided by the frame in which they were selected. Since all the sections of the thin foil perpendicular to the view plan were equivalent, the surface fraction was assumed equal to the volume fraction. A set of five TEM micrographs were used as suggested by DeHoff and Rhines [36].

The SANS experiments were performed on the PAXY spectrometer at the LLB (CEA-CNRS, Saclay, France, Proposal N° 12796) in the ORPHEE reactor. Two configurations of incident wavelength and sample-detector distance were used: 0.6 nm-2 m and 0.9 nm-5 m. The total covered scattering range was then $0.01 < q < 2$ nm^{-1}. Data were normalized and corrected for sample transmission and sample holder contribution. From the obtained 2D patterns, the

SANS intensities (I) were deduced. The analysis method (of the log(I) vs. q plots) in order to estimate the precipitate size and volume fraction has been widely presented in discussed in [37, 38].

Following this method, the SANS intensity per unit volume is given by:

$$I(q) = \Delta\rho^2 * N_p * V_p^2 * F(q) * s(q) \quad (1)$$

where N_p ,V_p and are the number density and volume of particles, respectively. $\Delta\rho^2$is the nuclear contrast and is written as :

$$\Delta\rho = \frac{b^p}{v_{at}^p} - \frac{b^m}{v_{at}^m} \quad (2)$$

Where $b^{p,m}$ and $v_{at}^{p,m}$ are the average scattering length and average atomic volume in the precipitate (p) or in the matrix (m), respectively. *F(q)* is the form factor of the particles and *S(q)* the structure factor (in the present study, the volume fraction is of the order of 1–2%, so *S(q)* is assumed equal to 1). The precipitates are supposed spherical with a radius *R* and the form factor corresponding is:

$$F(q,R) = \left[3\frac{\sin(qr) - qr\cos(qr)}{(qr)^3}\right]^2 \quad (3)$$

Furthermore, the precipitates are not monodisperse and a size distribution has to be considered. In this case, the Gaussian size distribution was taken into account for the data analysis. The Gaussian distribution is given by:

$$h(R) = \frac{1}{\sqrt{2\pi}\sigma} exp\left[-\frac{(R-R_m)^2}{2\sigma^2}\right] \quad (4)$$

where R_m is the mean radius. The half-width of the size distribution at half maximum is $\Delta R = \sqrt{2ln2}\sigma = 1.177\sigma$. Under these assumptions, equation (1) is rewritten as:

$$I(q) = \Delta\rho^2 * f_v * \frac{\int_0^\infty h(R) * V_p^2 F(q,R) * dR}{\int_0^\infty h(R) * V_p * dR} \quad (5)$$

Where f_v is the volume fraction of the particles.

3. Results and discussion

Figure 1 shows the microstructure of the Cu-Cr-Zr alloy in as-received state (Fig. 1a), after solution heat treatment at 1040 °C for 1 hour (Fig. 1b) and ECAP processing to one pass and subsequent aging at 550 °C for 4 hours (Fig. 1c–d). Figs. 1a and b were reproduced from EBSD maps in IQ (Index of Quality) format already published in [35].

As already reported in [35], the microstructure of the as-received alloy is characterized by the presence of long parallel elongated grains in fibrous form. This columnar structure with an average transverse grain size of about 130 μm results from strong thermal gradients during casting. Fig. 1b shows a coarse equiaxed granular microstructure that resulted after solution annealing at 1040 °C during 1 h in an argon atmosphere. This heating led to a grain mean diameter around 100 μm that is somewhat quite larger than that reported by Purcek et al. [31] in similar alloy that has underwent a solution annealed at 1020 °C for 20 min. This grain size difference is obvious owing to noticeable grain growth that may occur under higher temperature and longer annealing time. Grains boundaries are irregular and high quantity of annealing twins (see arrows) are present in the microstructure.

As can be observed in Fig.1c, ECAP processing to one pass and annealing at 550 °C for 4 h resulted in typical microstructure consisting of ultrafine sub-grains with average grain size about 200±40 nm estimated by the linear intercept method, in which all grains separated by both high-angle and low-angle grain boundaries (LAGBs) were taken into account.

This sub-grain size is very close to that reported by Purcek et al. [31] in Cu-0.8Cr-0.08Zr (wt.%) alloy after processing by ECAP technique up to 8 passes. These authors stated that the grain size and morphology did not considerably change between four and eight ECAP.

Hence, it can be stipulated that the sub-grain size saturates soon after one ECAP pass up to 16 pass. Fig.1b suggests that neither normal nor abnormal grain growth is observed in the aged alloy. A surprising absence of any effect of aging at 450 °C for 1 hour on the morphology and

grain size of ECAPed Cu–0.80Cr–0.080Zr (wt.%) alloy has been reported by Purcek et al. [27, 31]. Vinogradov et al. [5] demonstrated also the impressive fact that the ECAP structure remains fine-grained during heating and aging Cu-0.44Cr-0.2 Zr (wt.%) alloy at temperatures up to 600 °C. Most probably, this persistent UFG microstructure seems to be due to its effective stabilization by Cr cluster and/or Cu_5Zr particles [8].

Higher magnification shows that the microstructure (Fig. 1d) consists of dislocations-free sub-grains with sharp (high angle) boundaries and zones of moderate to high distortions and dislocations walls (low angle boundaries). Many grain boundaries are not clearly apparent due to the existence of high dislocation density in their vicinity. Many similar observations were reported in the literature after SPD processing and aging o Cu-based alloys [5, 28, 31].

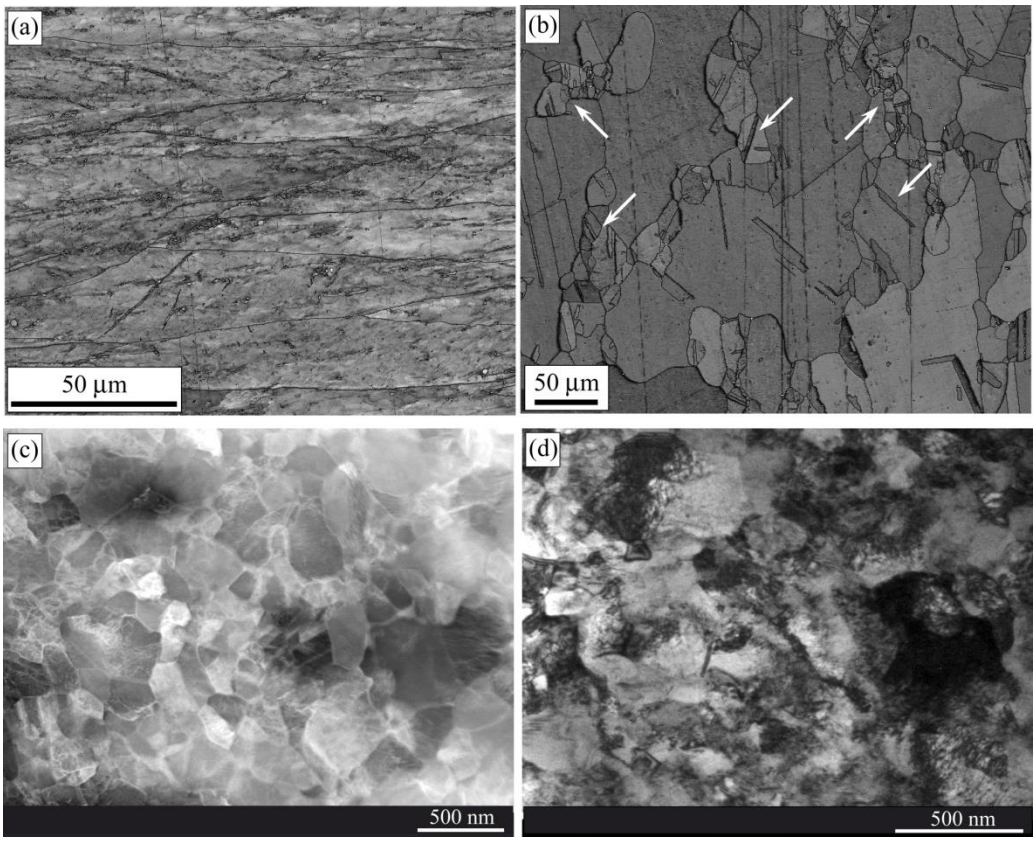

Fig.1. Microstructure of Cu-1Cr-0.1Zr (wt.%) alloy: a) As received, b) solution annealed at 1040 °C for 1 hour, HAADF-STEM (c) and TEM bright-field image (d) after ECAP processing to 1 pass and aging at 550 °C for 4h.

Normally, annealing in such conditions should result in substantial recrystallization and grain growth. In fact, previous work demonstrated that Cu-1Cr-0.1Zr (wt.%) alloy exhibits a very good thermal stability up to 550 °C after ECAP processing and annealing [22].

Interesting finding was the presence of quasi-cuboid and quasi-spheroid sub-micronic particles in the microstructure of annealed Cu-Cr-Zr alloy as shown in Fig.2a and Fig.2b. The size of cuboid and spheroid particles was about 380 and 620 nm respectively.

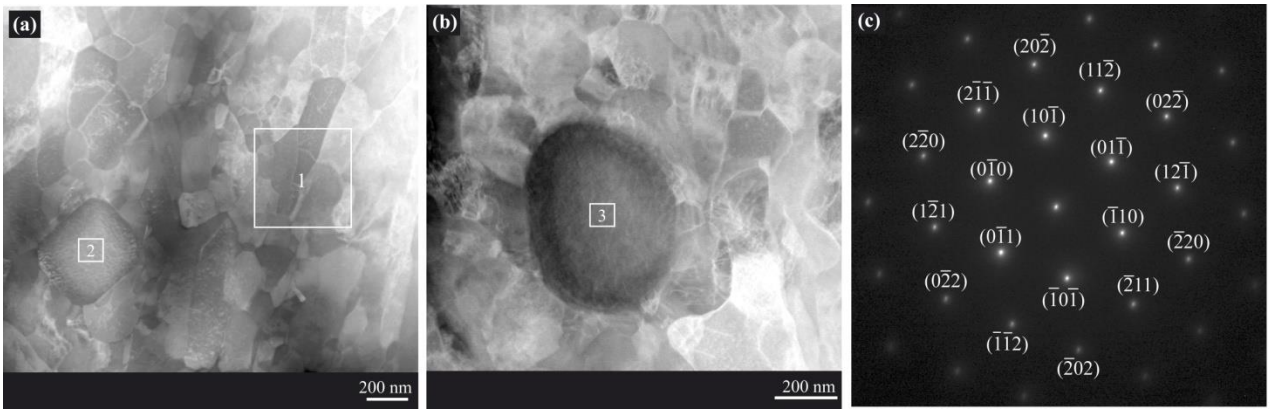

Fig.2. HAADF-STEM images of: a) Cuboid and b) spheroid sub-micronic Cr particles, c) Selected area diffraction (SAD) pattern taken from particle visible in Fig.2b.

Table 1 summarizes the results of point EDS analysis of Cu matrix, cuboid and the spheroid particles corresponding to analyzed zone 1, 2, and 3, respectively. As can be noticed the two particles are composed of ~ 98% of Cr and 2% of Cu. No trace of Zr element has been detected in the core of spheroid particle. The selected area diffraction (SAD) pattern taken from Fig.2b inside the sub-micronic precipitate is shown in Fig.2c. The key to Fig.2c (zone axis [111]) showing position of fundamental reflections from the Cr cluster, superimposed on the spots in Fig.2c, confirms the presence of only Cr bcc phase with lattice parameter of 0.2885 nm.

Table 1. EDS analysis of Cu matrix, cuboid and the spheroid particles.

	Cu Matrix	Cuboid particle	spheroid particle
Element	Weight %	Weight %	Weight %
Cr(K)	0.2	97.4	97.4
Cu(K)	99.7	2.5	2.5
Zr(K)	0.1	0.03	-

Besides the presence of rare sub-micronic particles in the microstructure, profuse nano-sized particles can be noticed inside the sub grains as demonstrated in Fig.3. Very similar observations were reported in the literature [5, 12, 32, 39, 40]. In these reports this particles were clearly identified as Cr clusters. Unfortunately, it was not possible to perform an EDS analysis because the precipitates are very small (few nanometers) compared to the foil thickness (usually about 50 nm). Hence, the EDS signal should be strongly convoluted between the particle and the matrix lying under and above particles. Vinogradov *et al.* [5] reported that the precipitation of fine Cr cluster started after aging at 375 °C for 15 h. The morphology and size of such clusters did not change appreciably and this latter remained in the range 5–20 nm diameter even after aging at 425 and 500 °C [5]. Meanwhile, it was reported that Cr clusters could be transformed to large and stable bcc particles at higher temperatures (500 °C) and longer annealing times (2 days) [38].

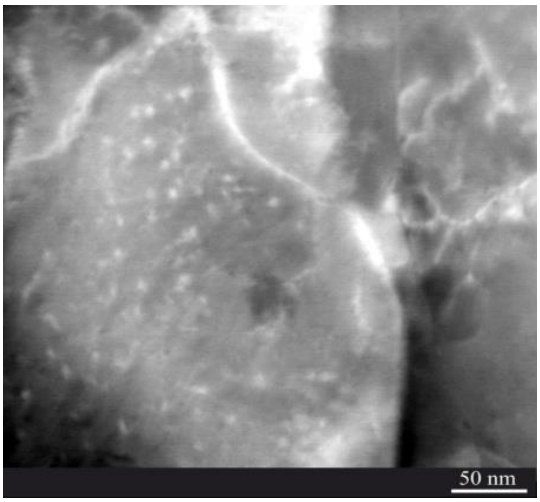

Fig.3. HAADF-STEM image showing nano-sized Cr clusters (in white contrast) within one sub-grain of deformed Cu-Cr-Zr alloy after annealing at 550 °C for 4h.

The precipitation nature and sequence in Cu-Cr-Zr alloys after thermomechanical processing was thoroughly studied [5–16], the presence of similar sub-micronic Cr clusters were reported in only very few reports [12, 41, 42]. Using energy-dispersive spectroscopy (EDS) mapping, Zhang et al. [42] have clearly shown that the sub-micronic Cr clusters have a core-shell structure with the shell of Zr and the core of Cr. These relatively coarse phases are thought to form during solidification and are left undissolved during solution [43]. The growth of coarse Cr phase in as cast ingot prefers along certain orientation [12]. Due to their relatively great size and very low volume fraction, SANS technique was unable to detect them within the explored q range in this study.

The nuclear scattering intensities measured on the deformed Cu-Cr-Zr alloy and annealed at 550 °C for 4 h are showing in Fig.4. Data from homogenized (un-processed and un-aged) Cu-1Cr-0.1Zr alloy as reference sample are also given for comparison. The nuclear scattering intensities of deformed Cu-1Cr-0.1Zr alloy and annealed at 550 °C for 4 h exhibit weak, extended and broad peak in the range $0.375 < q < 1.40$ nm^{-1} compared to the reference sample.

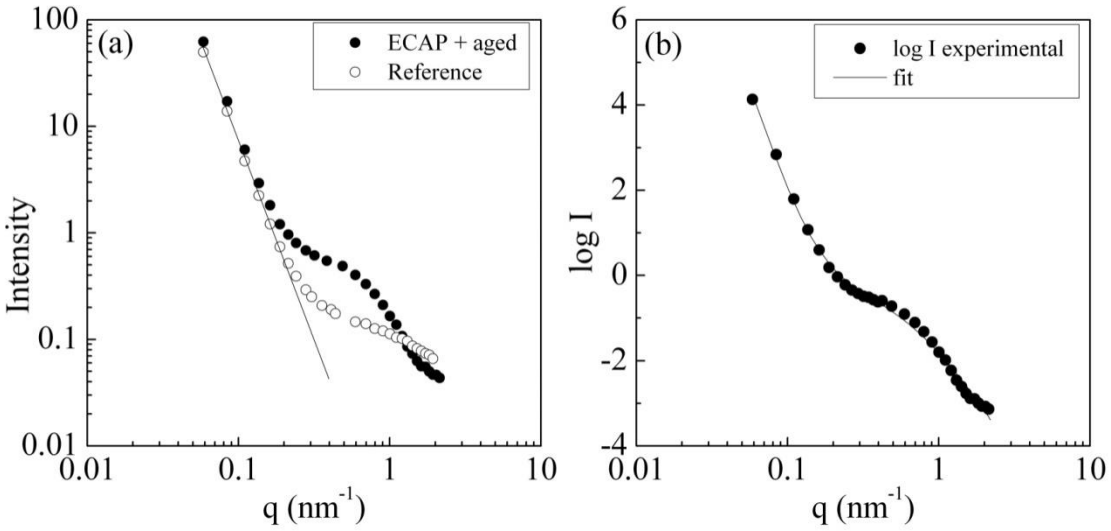

Fig.4. a) Nuclear scattering intensities for homogenized and deformed Cu-1Cr-0.1Zr alloy and annealed at 550 °C for 4 h, respectively. The continuous line illustrates the Porod behavior (I vs ($1/q^4$)) attempted for alloy without nano-particles and b) example of data adjustment obtained on the higher intensity.

The SANS data show that at small q, the intensity decreases rapidly following a slope in q^{-4}, this is consistent with a behavior of Porod which is the signature of the microstructure of a polycrystalline material with or without very large particles. The Porod behavior is the same for the reference and the ECAP plus aged sample; the microstructure (grains, grains boundaries or very large particles) was not modified by the last thermomechanical treatment. At high angle, that in the reference sample there is an additional contribution due to nano-objects; this contribution is much higher in the deformed and annealed material than in the reference. The measured scattered intensities were fitted assuming a Porod law and a Gaussian size distribution of small spherical or ellipsoidal particles. The agreement between the experimental and calculated data is very good as illustrated by the Fig.4 right. The results of the data fitting are summarized Table 2. The evaluation of the precipitated volume fraction

F_v from the experimental data fit requires knowing the nuclear contrast and thus the chemical composition. In this case, the precipitates are considered as pure Cr.

Table 2. SANS Cr precipitation characterization on homogenized and deformed Cu-1Cr-0.1Zr alloy and annealed at 550 °C for 4 h, respectively.

Sample	Mean radius (nm)	Standard deviation	F_v(%)
Reference	1.1	0.2	1.1
ECAP1P + 4 h at 550 °C	1.6	0.5	1.1

The results confirm that in the reference state, about 1% of very small particles already exists. In the annealed sample, the size of the precipitates has very clearly increased and reached 1.6 nm radius. The volume fraction is constant. In another hand, the size and volume fraction of nano-clusters of Cr were estimated by quantitative metallography from a set of HAADF-STEM micrographs (Fig.3, for example) and were compiled with those found by SANS in Table 3. As can be shown, both SANS and HAADF-STEM techniques allowed the assessment of the size and volume fraction of Cr clusters with reasonable accuracy and agreement.

In the literature, there is a controversy about the effect of long solution annealing on the Cr dissolution in the Cu matrix of Cu-Cr-Zr alloys. Indeed, many authors [18, 23, 44, 45] stated that Cu-Cr-Zr after solution annealing in the range 930-1050 °C is fully free from any precipitate or cluster. While other [12, 43, 46] evidenced the presence of Cr cluster due to their incomplete dissolution. Furthermore, the present results confirm the fact that SANS technique is a powerful method very sensitive to small variation of the nano-objects size.

Table 3. Estimation of size (diameter) and volume fraction of Cr nano cluster from SANS and HAADF-STEM analysis in of deformed Cu-Cr-Zr alloy after annealing at 550 °C for 4 h.

diameter (nm)		**F_v (%)**	
SANS	HAADF	SANS	HAADF
3.2	2.5	1.1	2.3

The size of Cr cluster (diameter 3.3–2.5 nm) as determined by SANS and HAADF-STEM fall within the range of those assessed by many authors [12, 18, 39, 40]. The volume fraction found by SANS is in agreement with the initial Cr content of the alloys, showing that all Cr atoms have precipitated. The F_v value determined by transmission electron microscopy is higher but remains on the one hand in the same order of magnitude, and on the other hand in the error bars of this technique. It is interesting to note that Chbihi et al. [32], using EDS mapping in the STEM mode, have estimated the Cr cluster volume fraction to be in the range 0.86–1.3%. Surprisingly, both techniques, did not evidence any presence of other types of precipitation. It has been demonstrated, using 3D-AP and TEM techniques, the presence of only bcc Cr clusters having probably Nishiyama–Wassermann (N–W) orientation relation after aging at 460 °C for 3 h and even after prolonged aging at 600 °C for 5 h of Cu–Cr–Zr alloy [20]. Chbihi et al [32] and Li et al. [40] reported also the existence of only Cr clusters. Li et al. [40] have identified them as having an ordered fcc with Cube-on-Cube relationship with the Cu matrix. From exhaustive TEM characterization, Chbihi et al [32] stated that three kinds of Cr clusters may coexist. Some of them are fcc and coherent with the matrix while others are probably bcc whether with N-W or Kurdjumov–Sachs (K-S) orientation relation.

Basing on TEM and 3D-APT, Chbihi et al [32] widely discussed the nucleation and growth of Cr clusters and have proposed a probable precipitation sequence as follows: (i) nucleation of coherent fcc spherical precipitates; (ii) growth and transformation of fcc spherical precipitates

into the bcc structure; and (iii) growth of bcc precipitates with a K-S–OR at the expense of those having an N-W–OR.

Hence precipitation of the Cr-rich equilibrium bcc phase was thought to initiate through the nucleation of fcc precipitates that are coherent with the Cu-rich fcc parent phase. Very similar precipitation scenario has been reported in age-hardenable Al-alloys [32]. Very recently, it has been demonstrated that the ordered fcc Cr phase is the precursor to the formation of the bcc in CuCrZr alloy [32].

The nature and morphology of intermetallic compounds that can form in Cu-Cr-Zr system has been considered to be linked to the local concentration of Zr. Intermetallics such as Cu_8Zr_3, $Cu_{51}Zr_{14}$, Cu_4Zr, Cu_5Zr as well as Heusler phases type ($CrCu_2$(Zr, Mg)) [19, 20], may precipitate in this system. However, close inspection of the published data revealed a preponderance of $Cu_{51}Zr_{14}$ compound when Cr content is less than <1% [12]. Such intermetallic particles generally have a larger size (d = 10-30 nm) than Cr precipitates [43]. Besides Cr clusters, Li et al. [40] have evidenced the presence of Cu_5Zr phase with quite smaller size (d <5 nm) that precipitated preferentially at twin boundaries, sub-grain boundaries and within the twin/matrix lamellae. These findings were in good agreement with previous observations if Holzwarth et al. [9] and Fuxiang et al. [47]. However, as mentioned above, very recently, Li et al. [40] reported the presence of only Cr cluster. It is worth noting that both SANS and HAAD/STEM techniques can only get the conclusion of the existence but not absence of precipitation with small size and small volume fraction.

The formation of Cu_xZr_y (mainly $Cu_{51}Zr_{14}$ and Cu_5Zr) should normally be enhanced after severe plastic deformation. As example, ECAP process can induce mutation in microstructure, in scale of grains as well as in precipitation, which can deviate greatly from paths that are observed in traditional processes. It has been stated that severe plastic deformation can be considered as “hot deformation at room temperature”, i.e. a balance

between deformation-induced grain refinement and deformation accelerated formation of equilibrium phases [48]. However, paradoxial inverse trends have also been reported in the literature. One of these processes reported in a number of experimental works is the spectacular cementite dissolution after [49] high pressure torsion (HPT).

Furthermore, it has been reported also that ECAP has a relatively complicated effect on the evolution of precipitates, and this effect is strongly dependent on the initial state of the aluminum alloy and the deformation temperature [50]. The dissolution of pre-existing precipitated phases and the formation of supersaturated solid solutions may also occur [50]. Straumal et al. [51] gave a review of all the possible effect of SPD processing on the phase transformation. They stated that, the phases before SPD and after this treatment are different. SPD can drive the formation or decomposition of a supersaturated solid solution, the dissolution of phases, disordering of ordered phases, amorphization of crystalline phases, synthesis of the low-temperature, high-temperature or high-pressure allotropic modifications, and nanocrystallization in the amorphous matrix.

Complementary on-going studies will be aimed to investigate thoroughly the whole nature and sequence of Cr clusters and precipitation and their evolution upon aging Cu-Cr-Zr system after severe plastic deformation by ECAP up to higher strains and aging.

4. Conclusions

Based on the experimental results, the following conclusions are drawn:

- Cu-1Cr-0.1Zr alloy exhibit a very good thermal stability up to 550 °C after ECAP processing with average grain size about 160 nm.
- HAADF-STEM evidenced the presence of cuboid and spheroid sub-micronic particle with size about 380 nm and 620 nm, respectively.

- SANS measurements allowed characterizing a very small precipitation in the reference alloy (2 nm diameter). The SANS and HAADF-STEM technics are in agreement on the ECAP then annealed sample exhibiting Cr particles of around 2.5 – 3.2 nm.
- The nano-precipitation of Cu_xZr_y was not evidenced within the aging conditions.

Acknowledgements

The authors wish to heartly thanks Prof. Jose Maria CABRERA from Polytecnica ETSEIB, Universidad Politécnica de Cataluña, for inviting and helping Miss K. ABIB during her several scientific stays.

References

[1] D.J. Edwards, B.N. Singh, S. Tähtinen, Effect of heat treatments on precipitate microstructure and mechanical properties of a CuCrZr alloy. J. Nucl. Mater. 367-370 (2007) 904–909. DOI: https://doi.org/10.1016/j.jnucmat.2007.03.064

[2] I.S. Batra, G.K. Dey, U.D. Kulkarni, S. Banerjee. Microstructure and properties of a Cu-Cr-Zr alloy. J. Nucl. Mater. 299 (2001) 91–100. DOI: https://doi.org/10.1016/S0022-3115(01)00691-2

[3] I.S. Batra, G.K. Dey, U.D. Kulkarni, S. Banerjee. Precipitation in a Cu-Cr-Zr. Mater. Sci. Eng. A 356 (2002) 32–36. DOI: https://doi.org/10.1016/S0921-5093(02)00852-3

[4] H. Fuxiang, M. Jusheng, N. Honglong,G. Zhiting, L. Chao, G. Shumei, Y. Xuetao, W. Tao, L. Hong, L. Huafen. Analysis of phases in a Cu-Cr-Zr alloy. Scr. Mater. 48 (2003) 97–102. DOI: https://doi.org/10.1016/S1359-6462(02)00353-6

[5] A.Vinogradov, V. Patlan, Y. Suzuki, K. Kitagawa, V.I. Kopylov. Structure and properties of ultra-fine grain Cu-Cr-Zr alloy produced by equal-channel angular pressing. Acta Mater. 50 (2002) 1639-1651. DOI: https://doi.org/10.1016/S1359-6454(01)00437-2

[6] Y. Zhang, A.A. Volinsky, H. Tran, Z. Chai, P. Liu, Ba. Tian, Y. Liu. Aging behavior and precipitates analysis of the Cu–Cr–Zr–Ce alloy. Mater. Sci. Eng. A 650 (2016) 248–253. DOI: https://doi.org/10.1016/j.msea.2015.10.046

[7] T. Kvačkaj, R. Bidulský, A. Kováčová, J. Ileninová, J. Bidulská. Analysis of metallic materials for iter with the emphasis on copper alloy. Acta Metallurgica Slovaca 20 (2014) 397–404. DOI: 10.12776/ams.v20i4.438

[8] D.V. Shangina, N.R. Bochvar, A.I. Morozova , A.N. Belyakov , R.O. Kaibyshev , S.V. Dobatkin. Effect of chromium and zirconium content on structure, strength and electrical conductivity of Cu-Cr-Zr alloys after high pressure torsion. Mater. Lett. 199 (2017) 46–49. DOI: https://doi.org/10.1016/j.matlet.2017.04.039

[8] P. Liu, J. Su, Q. Dong, H. Li. Microstructure and properties of Cu-Cr-Zr alloy after rapidly solidified aging and solid solution aging. J. Mater. Sci. Technol. 21 (2005) 475–478.

[9] U. Holzwarth, H. Stamm. The precipitation behaviour of ITER-grade Cu-Cr-Zr alloy after simulating the thermal cycle of hot isostaticpressing. J. Nucl. Mater. 279 (2000) 31–45. DOI: https://doi.org/10.1016/S0022-3115(99)00285-8

[10] N.Y. Tang, D.M.R. Taplin, G.L. Dunlop. Precipitation and aging in high-conductivity Cu-Cr alloys with additions of zirconium and magnesium. Mater. Sci. Technol. 1 (1985) 270–275. DOI: https://doi.org/10.1179/mst.1985.1.4.270

[11] P. Liu, B.X. Kang, X.G. Gao, J.L. Huang, B. Yen, H.C. Gu, Aging precipitation and recrystallization of rapidly solidified Cu–Cr–Zr alloy, Mater. Sci. Eng. A 265 (1999) 262–267. DOI : https://doi.org/10.1016/S0921-5093(98)01149-6

[12] H. Li, X. Shuisheng, M. Xujun, W. Pengyue. Phase and microstructure analysis of Cu-Cr-Zr. J. Mater. Sci. Technol. 23 (2007) 795–800.

[13] C.D. Xia, Y.L. Jia, W. Zhang, K. Zhang, Q.Y. Dong, G.Y. Xu, M. Wang. Study of deformation and aging behaviors of a hot rolled-quenched Cu-Cr-Zr-Mg-Si alloy during

thermomechanical treatments. Mater. Des. 39 (2012) 404–409. DOI: https://doi.org/10.1016/j.matdes.2012.03.003

[14] S.G. Mu, F.A. Guo, Y.Q. Tang, X.M. Cao, M.T. Tang. Study on microstructure and properties of aged Cu–Cr–Zr–Mg–RE alloy. Mater.Sci. Eng. A 475 (2008) 235–240. DOI: https://doi.org/10.1016/j.msea.2007.04.056

[15] P. Liu, B.X. Kang, X.G. Cao, J.L. Huang, B. Yen, H.C. Gu. Aging Precipitation and Recrystallization of Rapidly Solidified Cu-Cr-Zr-Mg Alloy. Mater. Sci. Eng. A 265 (1999) 262–267. DOI: https://doi.org/10.1016/S0921-5093(98)01149-6

[16] J.H. Su, P. Liu, Q.M. Dong, H.J. Li, F.Z. Ren, B.H. Tian. Recrystallization and Precipitation Behavior of Cu-Cr-Zr Alloy. J. Mater. Eng. Perform. 16 (2007) 490–493.https://doi.org/10.1007/s11665-007-9071-x

[17] Q.J. Wang, F. Liu, Z.Z. Du, J.Y. Wang. Hot-compression deformation behavior of Cu–Cr–Zr alloy. Chin. J. Rare Met. 37 (2013) 687–694. https://doi.org/10.1007/s11665-007-9071-x

[18] M. Hatakeyama, T. Toyama, J. Yang, Y. Nagai, M. Hasegawa, T. Ohkubo, M. Eldrup, B.N. Singh.3D-AP and positron annihilation study of precipitation behavior in Cu-Cr-Zr alloy. J. Nucl. Mater.386–388 (2009) 852–855.DOI:10.1016/j.jnucmat.2008.12.266

[19] J.P. Tu, W.X. Qi, F. Liu, Effect of aging treatment on the electrical sliding wear behavior of Cu–Cr–Zr alloy, Wear 49 (2002) 1021–1027. DOI: https://doi.org/10.1016/S0043-1648(01)00843-2

[20] W.X. Qi, J.P. Tu, F. Liu, Y.Z. Yang, N.Y. Wang, H.M. Lu, X.B. Zhang, S.Y. Guo, M. S. Liu, Microstructure and tribological behavior of a peak aged Cu–Cr–Zr alloy, Mater. Sci. Eng. A—Struct. 343 (2003) 89–96. DOI: https://doi.org/10.1016/S0921-5093(02)00387-8

[21] A. Vinogradov, Y. Suzuki, T. Ishida, K. Kitagawa and V. I. Kopylov. Effect of Chemical Composition on Structure and Properties of Ultrafine Grained Cu-Cr-Zr Alloys Produced by

Equal-Channel Angular Pressing. Mater. Trans. 45 (2004) 2187-2191. DOI: https://doi.org/10.2320/matertrans.45.2187

[22] K. Abib, H. Azzeddine, K. Tirsatine, T. Baudin, A. L. Helbert, F. Brisset, B. Alili, D. Bradai. Thermal stability of Cu-Cr-Zr alloy processed by equal-channel angular pressing. Mater. Charact. 118 (2016) 527–534. DOI: https://doi.org/10.1016/j.matchar.2016.07.006

[23] A. Vinogradov, K. Kitagawa, V.I. Kopylov. Fracture and Fatigue Resistance of Ultrafine Grain CuCrZr Alloy Produced ECAP. Mater. Sci. Forum 503-504 (2006) 811–816.DOI: https://doi.org/10.4028/www.scientific.net/MSF.503-504.811

[24] H. Azzeddine, B. Mehdi, T. Baudin, A.-L.Helbert, F. Brisset, D. Bradai, An in situ synchrotron X-ray diffraction study of precipitation kinetics in a severely deformed Cu-Ni-Si alloy, Mater. Sci. Eng. A 597 (2014) 288–294. DOI: https://doi.org/10.1016/j.msea.2013.12.092

[25] K.X. Wei, W. Wei, F. Wang, Q.B. Du, I.V. Alexandrov, J. Hu. Microstructure, mechanical properties and electrical conductivity of industrial Cu–0.5% Cr alloy processed by severe plastic deformation. Mater. Sci. Eng. A 528 (2011) 1478–484. https://doi.org/10.1016/j.msea.2010.10.059

[26] K.V. León, M.A.Muñoz-Morris, D.G.Morris. Optimisation of strength and ductility of Cu–Cr–Zr by combining severe plastic deformation and precipitation. Mater. Sci. Eng. A536 (2012) 181–189. https://doi.org/10.1016/j.msea.2011.12.098

[27] G. Purcek, H. Yanar, M. Demirtas, Y. Alemdag, D.V. Shangina, S.V. Dobatkin. Optimization of strength, ductility and electrical conductivity of Cu-Cr-Zr alloy by combining multi-route ECAP and aging. Mater. Sci. Eng. A 649 (2016) 114–122. https://doi.org/10.1016/j.msea.2015.09.111

[28] D.V. Shangina, J. Gubicza, E. Dodony, N.R. Bochvar, P.B. Straumal, N.Y. Tabachkova, S.V. Dobatkin. Improvement of strength and conductivity in Cu-alloys with the application of high pressure torsion and subsequent heat treatments. J. Mater. Sci. 49 (2014) 6674–6681. https://doi.org/10.1007/s10853-014-8339-4

[29] G. Purcek, H. Yanar, D.V. Shangina, M. Demirtas, N.R. Bochvar, S.V. Dobatkin. Influence of high pressure torsion-induced grain refinement and subsequent aging on tribological properties of Cu-Cr-Zr alloy. J. Alloys Compd. 742 (2018) 325–333. https://doi.org/10.1016/j.jallcom.2018.01.303

[30] M.J. Zehetbauer, Y.T. Zhu, (Eds.) Bulk Nanostructured Materials, Wiley-VCH, Weiheim, Germany, 2009.

[31] G. Purcek, H. Yanar, O. Saray, I. Karaman, H.J. Maier. Effect of precipitation on mechanical and wear properties of ultrafine-grained Cu–Cr–Zr alloy. Wear 311 (2014) 149–158. https://doi.org/10.1016/j.wear.2014.01.007

[32] A. Chbihi, X. Sauvage, D. Blavette. Atomic scale investigation of Cr precipitation in copper. Acta Materialia 60 (2012) 4575–4585. https://doi.org/10.1016/j.actamat.2012.01.038

[33] P. Staron, E. Eidenberger, M. Schober, M. Sharp, H. Leitner, A. Schreyer, H. Clemens. In situ small-angle neutron scattering study of the early stages of precipitation in Fe-25at% Co-9 at% Mo and Fe-1 at% Cu at 500 °C. Journal of Physics: Conference Series 247 (2010) 012038. DOI: 10.1088/1742-6596/247/1/012038

[34] K. Abib, F. HadjLarbi, L. Rabahi, B. Alili, D. Bradai. DSC analysis of commercial Cu−Cr−Zr alloy processed by equal channel angular pressing. Trans. Nonferrous Met. Soc. China 25 (2015) 838−843. DOI: 10.1016/S1003-6326(15)63671-8

[35] K. Abib, J. A. M. Balanos, B. Alili, D. Bradai.On the microstructure and texture of Cu-Cr-Zr alloy after severe plastic deformation by ECAP.Mater.Charact. 112 (2016) 252–258. DOI: https://doi.org/10.1016/j.matchar.2015.12.026

[36] R.T. DeHoff, F.N. Rhines, Quantitative Microscopy, McGraw-Hill Book company, (1968) p. 46.

[37] M.H. Mathon, C.H. DeNovion. De l'intensité à la structure des matériaux. I. Physique IV 9 (1999) 127–146.

[38] A. Maître, G. Bourguignon, G. Medjahdi, E. McRae, M. H. Mathon. Experimental study of L12 phase precipitation in the Pb–0.08 wt% Ca–2.0 wt% Sn alloy by resistivity and SANS measurements. Scr. Mater. 50 (2004) 685–689. DOI: 10.1016/j.scriptamat.2003.11.013

[39] X. Chen, F. Jiang, L. Liu, H. Huang, Z. Shi. Structure and orientation relationship of new precipitates in a Cu–Cr–Zr alloy. Materials Science and Technology. 34 (2017) 1–7. DOI: 10.1080/02670836.2017.1376428

[40] R. Li, E. Guo, Z. Chen, H. Kang, W. Wang, C. Zou, Tingju Li, T. Wang. Optimization of the balance between high strength and high electrical conductivity in CuCrZr alloys through two-step cryorolling and aging. Journal of Alloys and Compounds 771 (2019) 1044–1051. https://doi.org/10.1016/j.jallcom.2018.09.040

[41] H. Dybiec, Z. Rdzawski, M. Richert. Flow Stress and Structure of Age-hardened Cu-0.4 wt.% Cr Alloy after Large Deformation. Mater. Sci. Eng. A 108 (1989) 97–104. https://doi.org/10.1016/0921-5093(89)90410-3

[42] S.J. Zhang, R.G. Li, H.J. Kang, Z.N. Chen, W. Wang, C.L. Zou, T.J. Li, T.M. Wang. A high strength and high electrical conductivity Cu-Cr-Zr alloy fabricated by cryorolling and intermediate aging treatment. Mater. Sci. Eng. A 680 (2017) 108–114. https://doi.org/10.1016/j.msea.2016.10.087

[43] Z. Mei, L. Guobiao, W. Zidong, Z. Maokui. Analysis of precipitation in a Cu–Cr–Zr Alloy, China Foundry 5 (2008) 268–271.

[44] R.K. Islamgaliev, K.M. Nesterov, Y. Champion, R.Z. Valiev. Enhanced strength and electrical conductivity in ultrafine-grained Cu-Cr alloy processed by severe plastic

deformation. IOP Conf. Series: Materials Science and Engineering 63 (2014) 012118. DOI:10.1088/1757-899X/63/1/012118

[45] M. Lipinska, P.Bazarnik, M. Lewandowska. The electrical conductivity of CuCrZr alloy after SPD processing. IOP Conf. Series: Materials Science and Engineering 63 (2014) 012119. DOI:10.1088/1757-899X/63/1/012119

[46] G. Shuai, M. Zhang, Y. Yan. The effect of rare earth elements on Cr precipitations in a Cu-0.8 wt% Cr alloy. Image Anal.Stereol.23 (2004) 137–141. https://doi.org/10.5566/ias.v23.p137-141

[47] H. Fuxiang, M. Jusheng, N. Honglong, G. Zhiting, L. Chao, G. Shumei, Y. Xuetao, W. Tao, L. Hong, L. Huafen. Analysis of phases in a Cu–Cr–Zr alloy. Scr. Mater. 48 (2003) 97–102. https://doi.org/10.1016/S1359-6462(02)00353-6

[48] B.B. Straumal, A.A. Mazilkin, S.G. Protasova, S.V. Dobatkin, A.O. Rodin, B. Baretzky, D. Goll, G. Schütz. Fe–C nano grained alloys obtained by high-pressure torsion: Structure and magnetic properties. Mater. Sci. Eng. A 503 (2009) 185–189. https://doi.org/10.1016/j.msea.2008.03.052

[49] Y. Ivanisenko, W. Lojkovski, R.Z. Valiev, H.J. Fecht. The mechanism of formation of nanostructure and dissolution of cementite in a pearlitic steel during high pressure torsion. Acta Mater. 51 (2003) 5555–5570. https://doi.org/10.1016/S1359-6454(03)00419-1

[50] M. Gazizov, R. Kaibyshev. The precipitation behavior of an Al–Cu–Mg–Ag alloy under ECAP. Mater. Sci. Eng. A 588 (2013) 65–75. https://doi.org/10.1016/j.msea.2013.09.021

[51] B.B. Straumal, A.R. Kilmametov, Y. Ivanisenko, A.A. Mazilkin, O.A. Kogtenkova, L. Kurmanaeva, A. Korneva, P. Zieba, B. Baretzky. Phase transitions induced by severe plastic deformation: steady-state and equifinality. Int. J. Mater. Res. 106 (2015) 658–664. DOI 10.3139/146.111215